Optics Letters

Compact CWDM interleaver based on an interfering loop containing a one-dimensional Fabry–Perot cavity

Xinhong Jiang, Hongxia Zhang, Yong Zhang, Ciyuan Qiu, and Yikai Su*

State Key Lab of Advanced Optical Communication Systems and Networks, Department of Electronic Engineering, Shanghai Jiao Tong University, Shanghai 200240, China
**Corresponding author: yikaisu@sjtu.edu.cn*

Received 1 December 2017; revised 25 January 2018; accepted 25 January 2018; posted 26 January 2018 (Doc. ID 314340); published 26 February 2018

We propose and experimentally demonstrate a compact silicon photonic interleaver based on an interfering loop containing a 1D Fabry–Perot (FP) cavity for coarse wavelength division multiplexing (CWDM) applications. The interleaver consists of a directional coupler and a FP cavity designed to minimize the channel crosstalk. Instead of using an off-chip optical circulator, the reflection light of the interleaver can be separated from the input by placing two identical interleavers in a Mach–Zehnder interferometer (MZI) structure for practical applications. We also study the impacts of fabrication errors of the MZI structure. The fabricated device has a footprint of 64 μm × 70 μm and a channel spacing of ∼19 nm. The maximum crosstalk is −16 dB in a wavelength range from 1508 nm to 1590 nm.

OCIS codes: (130.3120) Integrated optics devices; (130.7408) Wavelength filtering devices; (230.5750) Resonators.

https://doi.org/10.1364/OL.43.001071

Coarse wavelength division multiplexing (CWDM) is a cost-effective solution for access area networks by using uncooled lasers [1]. Integrated CWDM filters have been demonstrated based on arrayed waveguide gratings (AWGs) [2,3] and planar concave gratings (PCGs) [4,5]. However, it is difficult to achieve both low insertion losses and flattop passbands in these devices. Optical lattice filters are preferred in solving these problems [6–8], which consist of multiple stages of interleavers [9–11], and cascaded Mach–Zehnder interferometers (MZIs) are needed in each interleaver to obtain flattop passbands. In our previous work, we proposed and experimentally demonstrated a compact silicon photonic interleaver consisting of an interfering loop that contains a Fabry–Perot (FP) cavity formed by two Sagnac loops [12]. The free spectral range (FSR) is ∼2 nm. To meet the channel spacing of CWDM, the FSR of the interleaver should be increased by using an FP cavity with a small cavity length. A 1D FP cavity formed by holes etched in a waveguide can be made ultra-compact with large FSR [13–15].

In this Letter, we propose and experimentally demonstrate a compact CWDM interleaver based on an interfering loop containing a FP cavity. To the best of our knowledge, it is the first demonstration of a flattop interleaver using a 1D FP cavity featuring a compact footprint and a large FSR. Since the interleaver has reflection light, two identical interleavers are embedded in an MZI structure to avoid the use of an off-chip circulator [16]. The footprint of the device is 64 μm × 70 μm. The measured transmission spectra have 4 channels with flattop passbands and a channel spacing of ∼19 nm.

Figure 1(a) shows the schematic of the proposed interleaver, which consists of a directional coupler and a FP cavity. The field transmission functions at ports T and R of the interleaver can be written as [12]

$$t_{\mathrm{T}} = a_1^2((t_1^2 - k_1^2)t_{\mathrm{FP}} + 2t_1k_1jr_{\mathrm{FP}}), \quad (1)$$

$$t_{\mathrm{R}} = a_1^2((t_1^2 - k_1^2)r_{\mathrm{FP}} + 2t_1k_1jt_{\mathrm{FP}}), \quad (2)$$

where t_{FP} and r_{FP} are the transmission and reflection functions of the FP cavity, respectively. t_1 and k_1 ($t_1^2 + k_1^2 = 1$) are the transmission and coupling coefficients of the directional coupler, respectively. $a_1 = \exp(-\alpha l_1 + j2\pi n_g/\lambda l_1)$ is the transmission factor of the waveguide, with l_1 denoting the length of the waveguides connecting the directional coupler and the FP cavity. α and n_g are the loss factor and the group index of the silicon waveguides, respectively. If t_1 is 0.924 [12], and

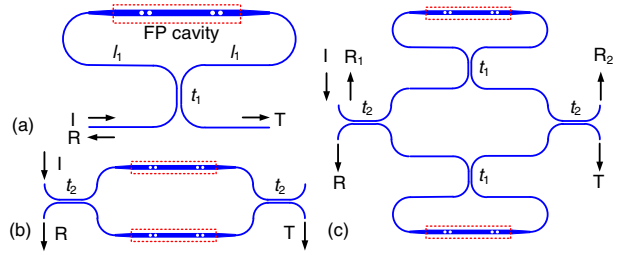

Fig. 1. (a) Schematic of the proposed interleaver. (b) MZI structure with the embedded FP cavities for measuring the reflection light. (c) The interleaver without a circulator for practical applications.

both $t_1^2 - k_1^2$ and $2t_1k_1$ are approximately 0.707, then Eqs. (1) and (2) can be simplified to

$$t_T = 0.707a_1^2(t_{FP} + jr_{FP}), \quad (3)$$

$$t_R = 0.707a_1^2(r_{FP} + jt_{FP}). \quad (4)$$

The crosstalk of the interleaver is determined by the maximum and minimum values of $|t_T|$ (or $|t_R|$), which are $0.707(|t_{FP}| + |r_{FP}|)$ and the absolute value of $0.707(|t_{FP}| - |r_{FP}|)$, respectively, under a lossless condition ($\alpha = 0$). Therefore, if the FP cavity is designed to satisfy $|t_{FP}| = |r_{FP}|$ at the central wavelengths of the CWDM channels, the maximum and minimum values are close to 1 and 0, respectively. Instead of using an off-chip optical circulator, the MZI structures shown in Figs. 1(b) and 1(c) can be used to measure the reflection spectrum of the FP cavity, and form the interleaver for practical applications, respectively. If the directional couplers of the MZIs are ideal 3-dB couplers ($t_2 = 0.707$), the transmission functions at ports T and R in Figs. 1(b) and 1(c) are jt_{FP}, jr_{FP}, jt_T, and jt_R, respectively. The following structural parameters are chosen based on our previously fabricated devices. The waveguide width and gap of the directional couplers are 0.45 μm and 0.2 μm, respectively. The coupling lengths for t_1 and t_2 are 4 μm and 11.5 μm, respectively. l_1 is 40 μm and the bend radius is 5 μm. 5-μm-long tapers are used to connect the 0.45-μm-wide waveguides and the FP cavities.

The commercial software Lumerical 2.5D variational finite-different time-domain (FDTD) is used to simulate the FP cavity and extract its scattering (S) parameters (S_{11} and S_{21}). Figure 2(a) presents the schematic of the FP cavity. The mirror section is optimized to satisfy the equation $|t_{FP}| = |r_{FP}|$ at the central wavelengths of the CWDM channels. The optimized mirror has two holes with a waveguide width of $w = 0.75$ μm. The radius and center-to-center distance of the holes are $r = 0.1$ μm and $a = 0.3$ μm, respectively. Figure 2(b) shows the transmission and reflection spectra of the designed mirror. It can be seen that the intensity reflectivity of the mirror is ~16%. Then l_2 is designed to be 14.129 μm to fit the ITU-T G.694.2 CWDM grids in a wavelength range from 1460 nm to 1620 nm. The nominal central wavelengths are 1471 nm, 1491 nm, 1511 nm, 1531 nm, 1551 nm, 1571 nm, 1591 nm, and 1611 nm. Figure 2(c) plots the simulated electric-field distribution of the FP cavity at a resonance wavelength of 1561 nm. Previously, birefringent crystal was used in a Sagnac interferometer-based flattop interleaver [17].

Once the S parameters of the FP cavity are obtained, they can be used to calculate the transmission and reflection spectra of the FP cavity, which are plotted in Fig. 3(a). To investigate the operation principle of the interleaver, we plot the phase differences $\Delta\Phi_T$ and $\Delta\Phi_R$ of the two terms in Eqs. (3) and (4), respectively, as shown in Fig. 3(b). Here $\Delta\Phi_T$ is the phase difference between t_{FP} and jr_{FP}, and $\Delta\Phi_R$ is the phase difference between r_{FP} and jt_{FP}. The phase differences are $2n\pi$ and $(2n+1)\pi$ alternatively (n is an integer), leading to alternative light construction and destruction. Since $|t_{FP}|$ is close to $|r_{FP}|$ at the central wavelengths of the CWDM channels, the amplitudes at the central wavelengths are approximately 1 or 0, meaning that a low crosstalk can be achieved. Figure 3(c) shows the simulated responses of the interleaver calculated by using Eqs. (3) and (4). The interleaver has eight channels in a wavelength range from 1460 nm to 1620 nm, with an insertion loss of ~0.3 dB and a channel spacing of ~20 nm. The simulated central wavelengths are 1472.9 nm, 1491.5 nm, 1510.4 nm, 1529.7 nm, 1549.8 nm, 1570.8 nm, 1592.0 nm, and 1609.5 nm, which show a maximum wavelength discrepancy of 1.9 nm from the nominal central wavelengths. In the passband at 1570.8 nm, the 1-dB, 3-dB, and 10-dB bandwidths are ~16.8 nm (0.42 FSR), ~21.0 nm (0.52 FSR), and ~27.8 nm (0.69 FSR), respectively. The 15-dB rejection bandwidth is ~11.7 nm (0.29 FSR). In Fig. 3(b), the phase difference $\Delta\Phi_T$ is ~3π near 1550 nm, which implies a destructive interference between t_{FP} and jr_{FP} according to Eq. (3).

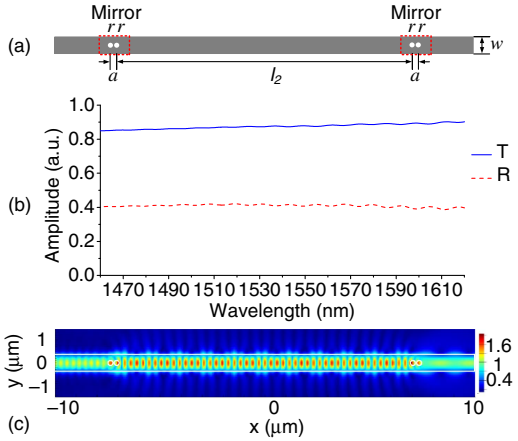

Fig. 2. (a) Schematic of the FP cavity. (b) Simulated transmission and reflection spectra of the mirror with two holes. (c) Simulated electric-field distribution of the FP cavity at a resonance wavelength of 1561 nm.

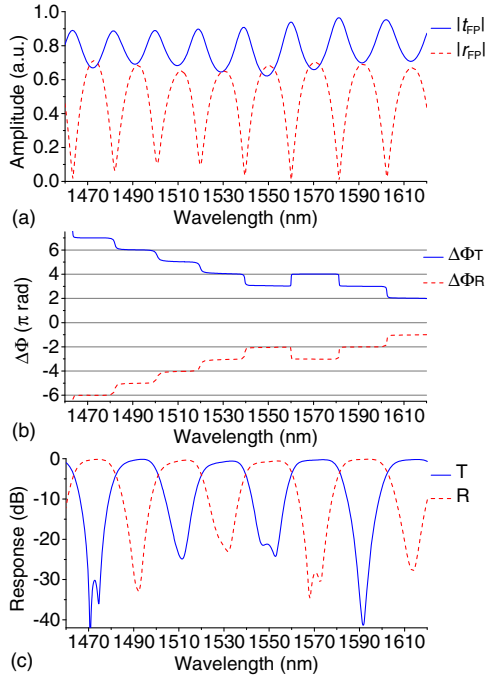

Fig. 3. (a) Simulated transmission and reflection spectra of the FP cavity. (b) Phase difference $\Delta\Phi_T$ of t_{FP} and jr_{FP}, and phase difference $\Delta\Phi_R$ of r_{FP} and jt_{FP}. (c) Simulated transmission and reflection spectra of the interleaver.

Since the spectra of $|t_{FP}|$ and $|r_{FP}|$ have two intersection points near 1550 nm in Fig. 3(a), there is a small bulge at 1550 nm in Fig. 3(c).

Fabrication errors of the MZI structure in Fig. 1(c) can degrade the device performances. Three types of fabrication errors are analyzed here [16]: (1) non-ideal 3-dB couplers, (2) unequal effective lengths of the MZI arms, and (3) unequal effective cavity lengths of the FP cavities. In an ideal case, the outputs at ports R1 and R2 are zero. For non-ideal 3-dB couplers, the response functions at ports R1, R, R2, and T are $T_{R1} = (t_2^2 - k_2^2)t_R$, $T_R = 2jt_2k_2t_R$, $T_{R2} = (t_2^2 - k_2^2)t_T$, and $T_T = 2jt_2k_2t_T$, respectively. For an effective length difference Δl_{MZI} of the MZI arms, we have $T_{R1} = (1 - \exp(j\Delta\varphi))/2t_R$, $T_R = j(1 + \exp(j\Delta\varphi))/2t_R$, $T_{R2} = (1 - \exp(j\Delta\varphi))/2t_T$, and $T_T = j(1 + \exp(j\Delta\varphi))/2t_T$, where $\Delta\varphi = \Delta l_{MZI} \times 2n_g\pi/\lambda$ and $n_g = \sim 4.35$ for the 0.45-μm-wide waveguide based on our previously fabricated devices. For an effective cavity length difference Δl_{FP} of the FP cavities, the response functions are $T_{R1} = (t_{R,1} - t_{R,2})/2$, $T_R = j(t_{R,1} + t_{R,2})/2$, $T_{R2} = (t_{T,1} - t_{T,2})/2$, and $T_T = j(t_{T,1} + t_{T,2})/2$, where $t_{R,1}$, $t_{T,1}$, $t_{R,2}$, and $t_{T,2}$ are the response functions of the interleaver with effective cavity lengths of l_2 and $l_2 + \Delta l_{FP}$, respectively.

Figure 4 shows the simulated responses at ports R1, R, R2, and T for the three types of fabrication errors. It can be seen that the responses at ports R and T do not have obvious changes. However, the outputs at ports R1 and R2 increase with the three types of fabrication errors. Based on the simulations, to obtain a crosstalk lower than −20 dB, the deviation of t_2 should be smaller than 0.035, the effective length differences Δl_{MZI} and Δl_{FP} need to be smaller than 12 nm and 24 nm, respectively. Fabrication-induced phase errors

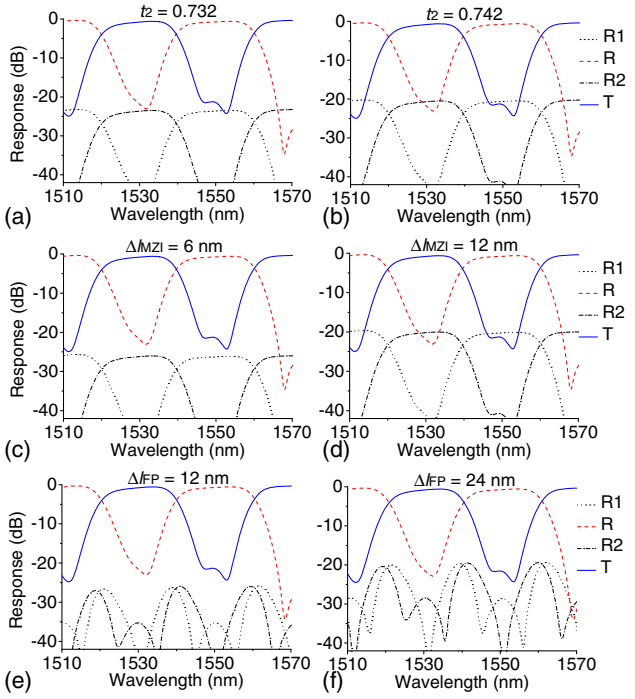

Fig. 4. Simulated responses at ports R1, R, R2, and T for three types of fabrication errors. (a) $t_2 = 0.732$. (b) $t_2 = 0.742$. (c) $\Delta l_{MZI} = 6$ nm. (d) $\Delta l_{MZI} = 12$ nm. (e) $\Delta l_{FP} = 12$ nm. (f) $\Delta l_{FP} = 24$ nm.

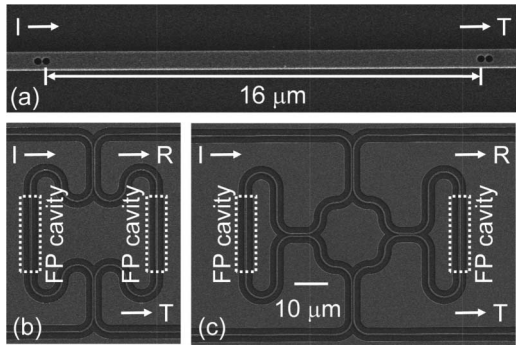

Fig. 5. SEM images of (a) the FP cavity, and (b), (c) the MZI structures with the embedded (b) FP cavities and (c) interleavers.

can be compensated by placing microheaters along the waveguides to form phase shifters.

The designed devices were fabricated on an SOI platform with a 220-nm-thick top silicon layer and a 3-μm-thick buried oxide layer. E-beam lithography (EBL, Vistec EBPG 5200) was used to define the device pattern. The top silicon layer was then etched by an inductively coupled plasma (ICP) etching process. A 1-μm-thick silica layer was deposited over the whole device as upper cladding by plasma enhanced chemical vapor deposition (PECVD). Figure 5 shows the scanning electron microscope (SEM) images of the FP cavity, and the MZI structures with the embedded FP cavities and interleavers. The footprint of the MZI structure with the embedded interleavers is 64 μm × 70 μm.

The transmission spectra of the fabricated devices were measured using a tunable laser (Keysight 81960A) and a power meter (Keysight N7744A) scanning from 1508 nm to 1590 nm with a step size of 5 pm. The TE grating couplers are employed to couple light into and out of the devices with a coupling loss of ∼7 dB/facet. To obtain a polarization-insensitive silicon photonic device, the polarization dependencies of the silicon waveguide need to be minimized by using square waveguides or polarization-diversity technology [18]. The dispersion can be compensated by using a dispersion compensator [19].

The transmission spectra of the devices are normalized to the transmission spectrum of a straight waveguide with grating couplers. The normalized transmission spectra of the MZI

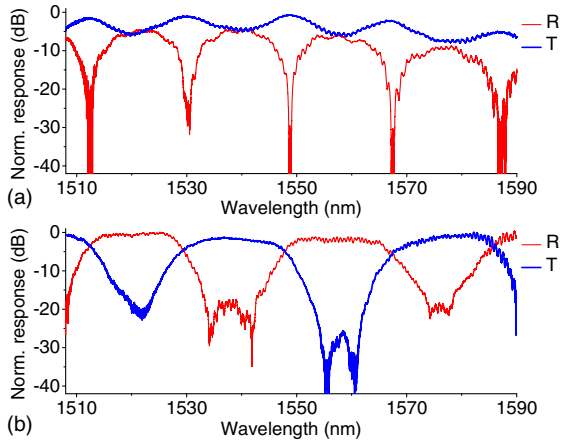

Fig. 6. Normalized measured transmission spectra of the MZI structures with the embedded (a) FP cavities and (b) interleavers.

Table 1. Comparisons of Integrated CWDM Filters

	Footprint (μm^2)	Spacing (nm)	IL (dB)	Crosstalk (dB)	BW_{1dB} (nm)
AWG [3]	305 × 260	22.3	~1.68	−20.6	~5
PCG [3]	250 × 155	20.2	~2.2	−23.3	~5
MZIs [11]	65 × 5 × 10^6	20	~0.5	−20 ~ −13	~14.1
MZIs [8]	40 × 100[a]	20	~0.5	−20	~16
This work	64 × 70[b]	19	~0.5	−24 ~ −16	~13

[a]The footprint of an interleaver in the multiplexer.
[b]The footprint can be further reduced to ~45 μm × 50 μm.

structure with the embedded FP cavities are shown in Fig. 6(a). At the central wavelengths, the differences between the transmissions at ports T and R are small, indicating low crosstalk. Figure 6(b) shows the transmission spectra of the MZI structure with the embedded interleavers, which has an insertion loss of ~0.5 dB and a channel spacing of ~19 nm. The channel spacing and the central wavelengths can be designed to fit the CWDM grids by varying the cavity length of the FP cavities. Since l_2 is much larger than a, the group index of the 0.75-μm-wide waveguide can be approximately calculated as $n_g = \lambda^2/(l_2 \times \mathrm{FSR})$. l_2 is 16 μm in the fabricated device, the FSR is ~38 nm, and the calculated group index of the 0.75-μm-wide waveguide at 1550 nm is n_g = ~3.95. In the passband at 1557.5 nm, the 1-dB, 3-dB, and 10-dB bandwidths are ~13 nm (0.34 FSR), ~19.7 nm (0.52 FSR), and ~26.4 nm (0.69 FSR), respectively. The 15-dB rejection bandwidth is ~10.8 nm (0.28 FSR). The experimental results show certain discrepancy from the simulation results, mainly in three aspects: (1) in Fig. 6(b), the crosstalk at the central wavelengths ranges from −24 dB to −16 dB, and the passband edges are asymmetric. These can be attributed to the wavelength dependencies of the directional couplers, which were not considered in the simulations. By employing broadband directional couplers [20,21] or multimode interferometer (MMI) couplers [22,23], the variation of crosstalk can be decreased. (2) The ripples might come from the fabrication imperfection of the holes and the reflection of the grating couplers. (3) The deviations of the resonance wavelengths come from the group index (n_g) difference of the 0.75-μm-wide waveguide between the FDTD simulation (n_g = ~4.25) and the fabricated device (n_g = ~3.95). The wavelength range of the measured transmission spectra is limited by the bandwidth of the grating couplers (a 3-dB bandwidth of ~20 nm). The fiber-to-fiber loss of the test setup is ~15 dB. In practical applications, edge coupling with low coupling loss and wide bandwidth [24] can be used.

The performance comparisons of various integrated CWDM filters are summarized in Table 1 (IL: insertion loss, $BW_{1\,dB}$:1 dB bandwidth). As can be seen from the table, the proposed interleaver features compact footprint, low insertion loss, and flattop passband. By removing the extra S-shaped waveguides connecting the 3-dB couplers and the interfering loops, the footprint can be further reduced to ~45 μm × 50 μm.

In conclusion, we have proposed and experimentally demonstrated a compact CWDM interleaver based on an interfering loop containing a one-dimensional FP cavity. The footprint of the device is 64 μm × 70 μm. The fabricated device has an insertion loss of ~0.5 dB and a channel spacing of ~19 nm. The maximum crosstalk is −16 dB at the central wavelengths. This interleaver features compact footprint, large FSR, low insertion loss, and flattop passbands.

Funding. National Key R&D Program of China (2016YFB0402501).

Acknowledgment. We thank the Center for Advanced Electronic Materials and Devices, Shanghai Jiao Tong University, for the support of device fabrication.

REFERENCES

1. "Spectral grids for WDM applications: CWDM wavelength grid," ITU-T Recommendation G.694.2 (2003).
2. C. Doerr, L. Chen, L. Buhl, and Y. Chen, IEEE Photon. Technol. Lett. **23**, 1201 (2011).
3. S. Pathak, P. Dumon, D. Van Thourhout, and W. Bogaerts, IEEE Photon. J. **6**, 4900109 (2014).
4. J. F. Song, Q. Fang, T. Y. Liow, H. Cai, M. B. Yu, G. Q. Lo, and D. L. Kwong, in *Optical Fiber Communication Conference* (Optical Society of America, 2011), paper JThA20.
5. G. Li, D. Lambert, J. Zyskind, J. Spann, M. Askari, G. Pickrell, M. Sodagar, and S. Krasulick, in *IEEE Conference on Group IV Photonics* (IEEE, 2016), p. 164.
6. M. Oguma, T. Kitoh, T. Shibata, Y. Inoue, K. Jinguji, A. Himeno, and Y. Hibino, Electron. Lett. **37**, 514 (2001).
7. S. Dwivedi, P. D. Heyn, P. Absil, J. V. Campenhout, and W. Bogaerts, in *IEEE Conference on Group IV Photonics* (IEEE, 2015), p. 9.
8. H. Xu and Y. Shi, IEEE Photon. Technol. Lett. **30**, 169 (2018).
9. M. Oguma, K. Jinguji, T. Kitoh, T. Shibata, and A. Himeno, Electron. Lett. **36**, 1299 (2000).
10. Q. Wang and S. He, J. Lightwave Technol. **23**, 1284 (2005).
11. T. Mizuno, M. Oguma, T. Kitoh, Y. Inoue, and H. Takahashi, IEEE Photon. Technol. Lett. **18**, 1570 (2006).
12. X. Jiang, Y. Yang, H. Zhang, J. Peng, Y. Zhang, C. Qiu, and Y. Su, J. Lightwave Technol. **35**, 3765 (2017).
13. J. S. Foresi, P. R. Villeneuve, J. Ferrera, E. R. Thoen, G. Steinmeyer, S. Fan, J. D. Joannopoulos, L. C. Kimerling, H. I. Smith, and E. P. Ippen, Nature **390**, 143 (1997).
14. Q. Quan and M. Loncar, Opt. Express **19**, 18529 (2011).
15. D. Yang, B. Wang, X. Chen, C. Wang, and Y. Ji, IEEE Photon. J. **9**, 4900412 (2017).
16. R. Soref and J. Hendrickson, Opt. Express **23**, 32582 (2015).
17. C. W. Lee, R. B. Wang, P. C. Yeh, and W. H. Cheng, Opt. Express **14**, 4636 (2006).
18. D. Dai, L. Liu, S. Gao, D. X. Xu, and S. He, Laser Photon. Rev. **7**, 303 (2013).
19. O. Schwelb, J. Lightwave Technol. **22**, 1380 (2004).
20. H. Morino, T. Maruyama, and K. Iiyama, J. Lightwave Technol. **32**, 2188 (2014).
21. C. Doerr, M. Cappuzzo, E. Chen, A. Wong-Foy, L. Gomez, A. Griffin, and L. Buhl, IEEE Photon. Technol. Lett. **17**, 1211 (2005).
22. D. Xu, A. Densmore, P. Waldron, J. Lapointe, E. Post, A. Delâge, S. Janz, P. Cheben, J. Schmid, and B. Lamontagne, Opt. Express **15**, 3149 (2007).
23. Z. Lu, D. Celo, P. Dumais, E. Bernier, and L. Chrostowski, in *IEEE Conference on Group IV Photonics* (IEEE, 2015), p. 57.
24. B. B. Bakir, A. V. De Gyves, R. Orobtchouk, P. Lyan, C. Porzier, A. Roman, and J. M. Fedeli, IEEE Photon. Technol. Lett. **22**, 739 (2010).